J. Fluid Mech. (1986), *vol.* 166, *pp.* 115–138
Printed in Great Britain

Thermals in extremely viscous fluids, including the effects of temperature-dependent viscosity

By R. W. GRIFFITHS

Research School of Earth Sciences, The Australian National University,
G.P.O. Box 4, Canberra A.C.T. 2601, Australia

(Received 21 May 1985 and in revised form 11 November 1985)

The flow induced by injection of a given amount of buoyancy or hot fluid from a localized source in a viscous fluid is investigated for conditions under which the Reynolds number Re is small compared with one, and the dimensionless buoyancy or Rayleigh number Ra is large compared with one. Laboratory experiments show that the buoyant fluid rises in the form of an extremely viscous 'thermal' which enlarges with time as a result of entrainment of surrounding fluid. The formation of a stable 'chemical ring' or torus of passive tracer similar in appearance to high Reynolds-number vortex rings is a notable feature of the creeping flow for high Rayleigh numbers. The possibility of large variations of viscosity due to temperature differences is included. A self-similar model is developed based on a boundary-layer analysis of a thin diffusive layer surrounding a spherical thermal for which the flow field is given by the exact solution for non-diffusive Stokes' flow. Experiments at $2.5 \times 10^2 < Ra < 2.5 \times 10^4$ and $Re < 10^{-2}$ demonstrate the nature of extremely viscous thermals, support the similarity solution and enable evaluation of a proportionality constant. Possible applications of the results to dispersion by viscous drops and particularly to thermal convection in the Earth's solid mantle are mentioned.

1. Introduction

The transport of heat away from heated or cooled horizontal boundaries by convection at large Rayleigh numbers ($> 10^5$) is recognized to be dominated by the intermittent motion of puffs of buoyant fluid away from the surfaces (Howard 1964; Elder 1968; Chu & Goldstein 1973; Sparrow, Husar & Goldstein 1970). The puffs of buoyant fluid are generally referred to as 'thermals' or 'mushroom' shaped structures. While most laboratory observations of such behaviour have been made using fluids with Prandtl numbers of order 10, recent experiments using high viscosity oils (Tritton 1985) indicate that similar intermittent, and even random, motions occur when the Prandtl number is as large as 10^5, conditions under which inertial forces associated with the convective motions are comparable to or less than the viscous forces. Similar intermittency and 'puffs' of buoyant fluid were seen in numerical experiments of high resolution at infinite Prandtl number (Jarvis 1984) (though this unsteadiness might have been the result of numerical instabilities). These are conditions relevant to thermal convection in the crystalline mantle of the Earth, where Reynolds numbers are expected to be, at greatest, 10^{-13}. However, little attention has been given to the dynamics or evolution of very viscous thermals. In the context of convection in the Earth's mantle, continuous plumes that would be produced by a steady release of buoyancy from a source region (as opposed to the

sudden release of a well-defined amount of buoyancy in the form of a thermal) have been postulated as a cause of intra-plate volcanism (Morgan 1971). Such plumes are generally considered to originate from fixed positions deep in the mantle, and probably from a hot, unstable boundary layer at the bottom of the mantle (e.g. Yuen & Schubert 1976; Loper & Stacey 1983). However, given a Rayleigh number of order 10^7 (based on the full depth of the mantle), it seems likely that such a boundary layer may well give rise to structures more closely described as intermittent thermals.

In order to learn more about the behaviour of thermals in Rayleigh–Bénard convection, this article considers the fundamental problem of the motion induced by a quantity of buoyancy initially released within a localized region in an unbounded and otherwise stationary fluid. The conditions of interest here are those under which the Reynolds number of the flow is small. The corresponding inviscid case has been studied extensively as a result of its relevance to a wide range of problems in fluid mechanics and, in particular, for its applications in meteorology (Scorer 1978). In the inviscid case, the buoyant material rises as a slightly oblate spherical 'thermal' inside which the flow is turbulent and outside which the flow is isothermal and irrotational. Turbulence is generated by the bulk rising motion driven by buoyancy and causes mixing of the buoyant material with the surrounding fluid (Morton, Taylor & Turner 1956; Turner 1957, 1964, 1973). Consequences of the turbulent entrainment are that the radius of the thermal increases as the square root of time, the rise velocity decreases as $t^{-\frac{1}{2}}$ and the temperature difference between the thermal and its environment decreases as $t^{-\frac{3}{2}}$ (Scorer 1957; Escudier & Maxworthy 1973; Turner 1973). The radius also expands linearly with distance travelled, with the half-angle ϕ of expansion given approximately by $\tan\phi = 0.25$. This angle is independent of the total buoyancy released (at least for cases in which no additional momentum is injected at the source) as the rate of entrainment is proportional to the rise velocity. The above similarity solution for vortex rings assumes, and experiments confirm, that thermals conserve their total buoyancy and thereby maintain their isolated nature.

Most work with laminar thermals has involved numerical simulations of the early stages in the development of thermals (e.g. Fox 1972). A notable exception is an analysis by Morton (1960) of the laminar motion produced by an extremely small quantity of buoyancy. The analysis consists of an expansion about the limit of zero Rayleigh number Ra, where $Ra = B/\kappa\nu_\infty$ is based on the injected buoyancy B, the thermal diffusivity κ and the ambient kinematic viscosity ν_∞. This approach therefore describes flow in which radial diffusion of heat dominates over advection. Similarity solutions of the momentum and heat equations require the radius and vertical position (z) of the thermal to scale with the diffusive length $(\kappa t)^{\frac{1}{2}}$ and predict a flow pattern similar to that for a turbulent thermal. However, there is no concentration of heat in the circular core of an extremely weak vortex ring. Furthermore, in contrast to the result $z \sim Ra^{\frac{1}{4}}t^{\frac{1}{2}}$ for turbulent thermals, Morton found that the height risen by weak thermals (in a fluid with Prandtl number $Pr = 1$) is directly proportional to the Rayleigh number. Schlien & Thompson (1975) carried out experiments with isolated laminar thermals in water ($Re \approx 20$) at large Rayleigh numbers ($Ra = 10^3$–10^4), and found that the flow was approximately self-similar, though only a small amount of data was collected.

Returning to convection at large Rayleigh number of a large Prandtl number fluid above a heated boundary, we note that intermittent instability of a thin thermal boundary layer will produce thermals or plumes that are likely to have length scales and density anomalies comparable to the thickness and density difference across the boundary layer. Since the boundary layer becomes unstable when a local Rayleigh

number based on these same parameters exceeds a critical value (Howard 1964), we conclude that this critical value provides a reasonable first estimate of the Rayleigh number for the thermal. For a fluid of constant viscosity the critical Rayleigh number is close to 10^3, but may be smaller if the hot boundary layer has a reduced viscosity. Slightly larger Rayleigh numbers for thermals would be achieved if each thermal drew hot fluid from close to the boundary over a finite growth period (Sparrow *et al.* 1970). Thus thermals in creeping flow are not always 'weak' in the sense considered by Morton (1960), but can have large Rayleigh numbers at which the transport of heat is dominated by advection rather than diffusion.

Viscous thermals are also of interest in the field of chemical engineering, where the shape of, and heat and mass transfer from, buoyant drops has been widely investigated. However, it appears that exchange by molecular diffusion between the drop and its surroundings has been discussed only for the case of immiscible (spherical) drops (Kronig & Brink 1951; Pan & Acrivos 1968; Brignell 1975), while the behaviour of miscible drops in Stokes flow, coupled with diffusion of buoyancy, has not been considered beyond a single interesting observation by Kojima, Hinch & Acrivos (1984). These authors noted that when a drop of cold viscous liquid fell into a warmer, less dense environment with a Reynolds number less than one, it opened into a thin spherical cap with a mushroom-like appearance, an evolution entirely different from that observed for isothermal drops. In this and a subsequent paper (Griffiths 1986*a*) I will explain this behaviour.

An additional important parameter to be included in this investigation is a viscosity difference between the drop and its environment. A rapid decrease of viscosity with increasing temperature is a notable property of almost all fluids with large Prandtl number, and particularly of geological materials. Previous approaches to the investigation of the motion of hot buoyant material through fluids with temperature dependent viscosities have concentrated largely on the problem of a hot rigid body moving under a given force or at a given velocity (Marsh 1982, 1984; Marsh & Kantha 1978). When the driving force is sufficiently small, flow about the hot body is confined to a thin, mobile low-viscosity boundary layer that lubricates the motion of the body (Morris 1982; Ribe 1983). Excepting for the latent heat effects on melting, this limiting case is equivalent to that in which a hot body melts its way through an otherwise solid and rigid environment. At the other extreme, when the driving force is sufficiently large, such a thin boundary layer is not capable of transporting sufficient material, the surrounding high-viscosity fluid deforms, and the flow around the rigid body is that expected for a fluid of uniform viscosity (Stokes limit). I point out here that lubricating boundary-layer flow around a rigid body or a fluid drop can occur only when the body is driven predominantly by an intrinsic density difference (resulting from a difference in chemical composition) and not when the buoyancy results primarily from temperature differences. The dominance of compositional buoyancy is implicitly assumed in the analyses of Marsh & Kantha and Morris, and in the experiments of Ribe, as these authors neglect the thermal buoyancy of the hot fluid in the thermal boundary layer as well as the influence of the buoyancy acquired by all the fluid that has already passed through the boundary layer. Thus the subject of this paper can be viewed as the opposite limit: motion driven by thermal buoyancy alone. For this case, there is no pressure gradient available to force the buoyant low-viscosity boundary layer material from the front to the rear of the mass of buoyant material; rather it is dragged to the rear by viscous stresses. It will be shown that the effects of large viscosity variations are therefore minor and readily taken into account.

A model and similarity solution for high Rayleigh number viscous thermals is presented in §2. Experiments with isolated thermals in viscous oils are described in §§3 and 4, and the measurements compared with the similarity solution in §5. Conclusions drawn from the comparison are discussed in §6.

2. A boundary layer analysis for thermals with large Rayleigh number

Consider a volume V_0 of hot fluid at temperature T_0 and dynamic viscosity μ_0 placed in an unbounded, initially uniform environment of the same fluid with temperature T_∞ and viscosity μ_∞ far from the hot region. We assume the density to be given by the linear equation of state

$$\rho = \rho_\infty[1-\alpha(T-T_\infty)], \tag{1}$$

and that the viscosity is a function of temperature only, generally decreasing as the temperature increases. There are initial temperature and density anomalies $\Delta T_0 = T_0 - T_\infty$ and $\Delta\rho_0 = \rho_\infty \alpha \Delta T_0$, respectively, and a net initial buoyancy $B_0 = g\Delta\rho_0 V_0/\rho_\infty$, where g is the acceleration due to gravity. A Rayleigh number for the flow is defined as

$$Ra = \frac{g\alpha\Delta T_0 V_0}{\kappa\nu_\infty} = \frac{B_0}{\kappa\nu_\infty}, \tag{2}$$

where κ is the thermal diffusivity (assumed constant) and $\nu_\infty = \mu_\infty/\rho_\infty$ is the kinematic viscosity far from the source of buoyancy. This formulation applies equally to systems in which a volume of hot fluid is emplaced and to those in which heat alone is injected. The conditions of interest throughout this paper are those under which $Ra \gg 1$ but a Reynolds number for the flow is very much less than one.

Before discussing the subsequent flow it is useful to begin by recalling some features of creeping flow for the case in which there is no diffusion of buoyancy (the limit $Ra = \infty$). The flow is then reversible and the bulk rising motion of the buoyant material is described by Stokes' law. When the buoyant fluid itself has a uniform density and viscosity, an exact result is that the sphere is the only compact steady geometry, there being zero normal stress everywhere on the outer surface (Batchelor 1967; Kojima *et al.* 1984†). Hence, the buoyant fluid, once it reaches a steady form, takes the shape of a spherical bubble. The structure of the flow is sketched in figure 1(*a*). The sphere rises against gravity at a velocity

$$U = \frac{1}{12}\frac{g\Delta\rho D^2}{\rho_\infty \nu_\infty} f\left(\frac{\mu}{\mu_\infty}\right), \quad f = \frac{1+\mu/\mu_\infty}{1+1.5\mu/\mu_\infty}, \tag{3}$$

where $\Delta\rho$ is the density deficit for the bubble relative to ρ_∞, D is the diameter of the bubble and μ is the viscosity inside the bubble (Lamb 1932). This velocity decreases slightly with increasing viscosity ratio, with $f = 1$ at $\mu \ll \mu_\infty$, $f = \frac{2}{3}$ at $\mu = \mu_\infty$, and $f = \frac{2}{3}$ at $\mu \gg \mu_\infty$. In the non-diffusive case there is no instability on the spherical boundary and no mixing of fluids, even though surface tensions are assumed to be zero and the fluids miscible.

On the other hand, diffusion of heat into the surrounding fluid may be significant in the real flow. As a result, the flow is irreversible and no longer symmetric about the horizontal plane through the centre of the bubble. The distribution of heat is then no longer steady. At large Rayleigh numbers the diffusion of heat must be confined

† These authors showed that not even a toroidal ring of buoyant fluid is a steady solution in creeping flow.

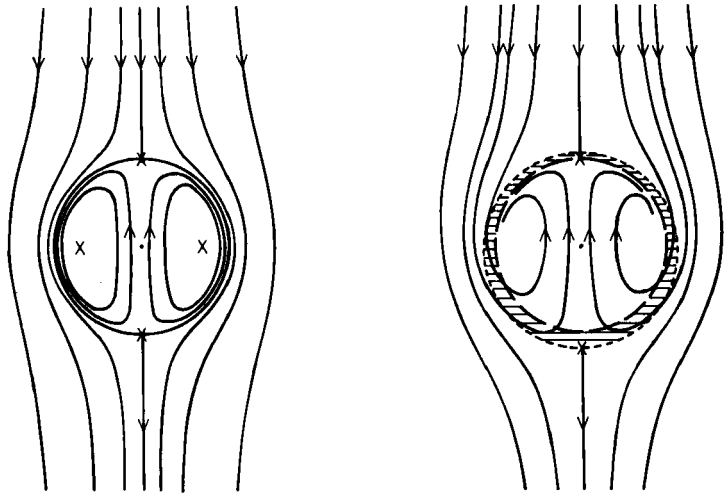

(*a*) (*b*)

FIGURE 1. Sketch of (*a*) the analytically derived steady streamlines in and around a bubble of buoyant fluid rising with small Reynolds number when the flow is reversible and (*b*) the model paths of fluid particles for the case in which buoyancy diffuses into a boundary layer. Streamlines are relative to the coordinate system moving with the centre of the bubble. The steady streamlines (*a*) are also the stream function for the unsteady flow in (*b*). In (*b*) the dotted circle shows the boundary of the buoyant fluid, the hatched region is the thermal boundary layer, and the inner broken circle represents the size of the bubble at a time of order a/U earlier.

to a thin boundary layer similar to that which forms around a rigid or immiscible drop (e.g. Brignell 1975; Pan & Acrivos 1968). The expected nature of the flow is sketched in figure 1(*b*), where it is assumed that the presence of a thin buoyant thermal boundary layer will not significantly alter the spherical shape realized in the reversible flow. Furthermore, since time-dependent terms in the momentum equation for creeping flow are negligible, the unsteady motion is at any time the same as steady Stokes flow, in this case flow past a sphere†.

As it is heated, the material in the boundary layer becomes indistinguishable from fluid already inside the thermal. The newly heated material is buoyant and will tend to take part in the rising motion to an extent that depends upon the relative magnitudes of local viscous forces ($\nu\nabla^2\boldsymbol{u}$) and buoyancy forces ($g\Delta\rho/\rho_\infty$). Noting that velocity gradients are small as a result of rapid diffusion of vorticity ($\nu\nabla^2\boldsymbol{u} \ll \nu_\infty U/D^2$), the ratio r of local buoyancy to viscous forces can be written as $r \gg \Delta\rho D^2/\rho_\infty \nu_\infty U$. With the velocity scale (3), this ratio satisfies $r \gg 1$. Thus it seems that there is a strong tendency for the thin heated boundary layer to rise with the thermal rather than to be pulled away by viscous stresses into a warm trail‡. So long as the circulation velocity within the thermal is comparable to U (a condition that holds when $\mu \leqslant \mu_\infty$), and the scale of the boundary layer is small compared with D, the newly heated

† Taking the velocity of the thermal to be that for a spherical bubble, the Péclet number becomes $Pe = UD/\kappa = Ra/2\pi$ and the Reynolds number becomes $Re = UD/\nu_\infty = Ra/2\pi Pr$. Hence flow with $Re \ll 1$ requires $Ra \ll 2\pi Pr$, where Ra is defined in (2).

‡ Kojima *et al.* (1984) show that there is no continuous enlargement of a buoyant torus due to viscous entrainment at zero Reynolds number, but that a torus grows by viscous entrainment of surrounding fluid when terms of first order in Re are included. Thus viscous stresses tend to encourage entrainment rather than detrainment.

material will rise along the axis of the thermal (as shown in figure 1*b*), despite being cooler than the rest of the thermal. Of course, some heat contained in an exponential temperature profile in the outer wing of the boundary layer may be swept away from the thermal. This heat loss may be small but its importance must be tested by laboratory experiments. The entrainment process can also be viewed in terms of a dividing particle path that approaches the rear stagnation point of a thermal in the coordinate system moving with the thermal. At this stagnation point in a reversible flow, radial stresses vanish. However, fluid approaching that same point in the diffusive case must be buoyant, and will rise. Hence the stagnation point and dividing particle path are likely to be displaced to a larger radius that will encompass most of the buoyant boundary layer. Once the newly heated material is wrapped around within the thermal, any remaining temperature and viscosity difference will be removed by further thermal diffusion. Thus I will assume that temperature and viscosity are almost uniform within the spherical region.

For large Rayleigh numbers, the thickness δ of the diffusive boundary layer is small ($\delta \ll D$) and scales as

$$\delta = k_1 \left(\frac{\kappa D}{U}\right)^{\frac{1}{2}}, \tag{4}$$

where D/U is the timescale for material to pass around the thermal and k_1 is a numerical factor. The rate of increase of the volume of hot material can be written as

$$\dot{V} = k_2 UD\delta, \tag{5}$$

where k_2 is a second numerical factor. Combining (4) and (5) gives

$$V = k_1 k_2 U^{\frac{1}{2}} D^{\frac{3}{2}} \kappa^{\frac{1}{2}}. \tag{6}$$

The velocity U is given by Stokes' law (3).

At this stage we make the important simplifying assumption that all of the hot boundary layer is entrained, causing the total buoyancy B_0 in the thermal to be conserved†. Thus

$$\Delta\rho V = \Delta\rho_0 V_0. \tag{7}$$

Eliminating the density anomaly from (7) and (3) leads to an expression for the instantaneous velocity:

$$U = \frac{f}{2\pi} Ra\kappa/D, \tag{8}$$

where the Rayleigh number is constant in time. Substitution of (8) into (6) gives the differential equation

$$D\dot{D} = k_1 k_2 \left(\frac{2}{\pi^3}\right)^{\frac{1}{2}} \kappa\, Ra^{\frac{1}{2}} f^{\frac{1}{2}}. \tag{9}$$

The function $f(\mu/\mu_\infty)$ will generally vary with time. However, it is constant if the viscosity is uniform or if $\mu \ll \mu_\infty$ throughout the period of interest. In the worst case, f may change from 1.0 to 0.8 as the thermal rises and cools. The factors k_1 and k_2 are constant if the flow is assumed to be self-similar at all times. Solving (9) with f constant, and applying the simplest and most enlightening initial condition $D = 0$ at $t = 0$, we find

$$\frac{D}{D_0} = C\, Ra^{\frac{1}{4}} \frac{(\kappa t)^{\frac{1}{2}}}{D_0}, \tag{10}$$

† This assumption can be relaxed by allowing a partition of the boundary-layer heat flux into a portion remaining within the thermal and a portion left behind in a wake. The resulting similarity solution then involves two unknown constants. This approach is not presented, as (7) leads to an adequate description of the data.

where the numerical constant $C = (k_1 k_2)^{\frac{1}{2}} (8f/\pi^3)^{\frac{1}{4}}$. Hence, the rate of increase of diameter with *time* as given by (10) is greater for larger Rayleigh numbers. At the same time, the boundary-layer thickness given by (4), (8) and (10), $\delta \sim Ra^{-\frac{1}{4}}(\kappa t)^{\frac{1}{2}}$, is smaller for larger Rayleigh numbers. This result is equivalently written as $\delta/D \sim Ra^{-\frac{1}{2}}$ and is identical to that found for diffusive boundary layers around immiscible drops (Brignell 1975). This similarity can be extended to show that, as a consequence of the shape of the circulation within the sphere, the boundary layer diverges as it approaches the axis at the rear to form a broader region of width $\sim D\,Ra^{-\frac{1}{4}}$ within the upward axial flow.

Equation (10) is written in dimensionless form using the lengthscale $D_0 = (6V_0/\pi)^{\frac{1}{3}}$, the diameter of a sphere of volume V_0, and the timescale D_0^2/κ for thermal diffusion. However, a timescale that more usefully characterizes the flow is $D_0/U \sim D_0^2/\kappa Ra$, the time taken by the thermal to move through one diameter. Then (10) is better written as

$$\frac{D}{D_0} = C\,Ra^{-\frac{1}{4}}\left(\frac{Ra\kappa t}{D_0^2}\right)^{\frac{1}{2}}. \tag{11}$$

Substituting (11) into (8) gives the dimensionless velocity

$$\frac{UD_0}{\kappa Ra} = \frac{f}{2\pi C} Ra^{\frac{1}{4}}\left(\frac{Ra\kappa t}{D_0^2}\right)^{-\frac{1}{2}}. \tag{12}$$

Hence, the velocity decreases with time as a result of dilution and cooling of the thermal. The velocity decrease is a result of the requirement that the viscous drag on the enlarging thermal must remain constant in order to balance the net driving force provided by the constant buoyancy. On integrating (12) over time, with the centre of the thermal lying at $z = 0$ when $t = 0$, the vertical distance travelled is

$$\frac{z}{D_0} = m\left(\frac{Ra\kappa t}{D_0^2}\right)^{\frac{1}{2}}, \quad m = \frac{f}{\pi C} Ra^{\frac{1}{4}}. \tag{13}$$

Hence, the distance travelled in dimensional terms is proportional to $Ra^{\frac{3}{4}}$, a behaviour significantly different from that of both turbulent thermals (Scorer 1978) and Morton's (1960) extremely weak thermals.

From (11) and (7), the temperature (and density) anomaly decreases with time according to

$$\frac{\Delta T}{\Delta T_0} = C^{-3} Ra^{\frac{3}{4}}\left(\frac{Ra\kappa t}{D_0^2}\right)^{-\frac{3}{2}}. \tag{14}$$

Note that this similarity solution has no physical meaning near the virtual origin $t = 0$, $z = 0$, where $\Delta T \to \infty$ and the density in the thermal becomes negative.

All of the variables may be expressed as functions of the height to which the thermal has risen by combining (13) with (11), (12) and (14). Thus

$$\frac{D}{D_0} = 2\epsilon\left(\frac{z}{D_0}\right), \quad \epsilon = \frac{\pi C^2}{2f} Ra^{-\frac{1}{2}}, \tag{15}$$

$$\frac{UD_0}{\kappa Ra} = \frac{f^2}{2(\pi C)^2} Ra^{\frac{1}{2}}\left(\frac{z}{D_0}\right)^{-1}, \tag{16}$$

$$\frac{\Delta T}{\Delta T_0} = \left(\frac{f}{\pi C^2}\right)^3 Ra^{\frac{3}{2}}\left(\frac{z}{D_0}\right)^{-3}. \tag{17}$$

Hence the diameter increases linearly with distance from the virtual origin with a half-angle of expansion ϕ given by $\tan^{-1}\phi = \epsilon$. The constant C must be determined

from experiments. The dependence of ϵ on Ra in (15) is again different from that found for turbulent thermals with large Reynolds numbers, for which ϵ is approximately independent of the total buoyancy, and from that for the limit $Ra \to 0$, where $\epsilon \sim Ra^{-1}$.

Finally, the position of the virtual origin $z = t = 0$, at which $D = 0$ and $U \to \infty$, is related to the length scale D_0. From (11) and (13),

$$t_0 = \left(\frac{Ra^{\frac{1}{2}}}{C^2}\right)\left(\frac{D_0^2}{\kappa Ra}\right), \quad z_0 = \frac{f}{\pi}\left(\frac{Ra^{\frac{1}{2}}}{C^2}\right)D_0, \tag{18}$$

where t_0 and z_0 are the time and position (measured from the virtual origin) at which $D = D_0$.

3. Experimental apparatus and method

3.1. *The fluids*

For the experiments reported here (and for related experiments involving both chemical and thermal density contrasts) it was desirable to use viscous liquids that possessed a number of qualities making handling, observations and measurements practical, while making accessible a combination of large Rayleigh numbers and small Reynolds numbers. The latter requirement constrains the Prandtl number to $Pr \gg Ra/2\pi$ (see footnote in §2). Thus, in order to use $Ra \sim 10^4$ while maintaining $Re \ll 1$, a liquid with $Pr \gg 2 \times 10^3$ is required.

The liquids chosen are two members of a range of artificial polybutene oils manufactured by BP Chemicals Ltd. The 'Hyvis' range provides transparent, odourless and non-irritating oils with viscosities (at 20 °C) between 1 and 10^5 cm^2 s^{-1}. 'Hyvis 3', with a nominal viscosity at 20 °C of 10^2 cm^2 s^{-1} was used in most experiments, while 'Hyvis 30', with its nominal viscosity of 10^3 cm^2 s^{-1}, was employed to give the smallest Rayleigh numbers without unduly reducing the total buoyancy (or lengthscale). Viscosities of these oils were measured at 5 °C intervals between 10° and 85 °C using capillary tube viscometers. The resulting curves of viscosity as a function of temperature are shown in figure 2 and have a precision better than 1 %. The viscosities vary much more rapidly than exponentially. Densities were measured to an accuracy of 10^{-4} g cm^{-3} at 20°, 30°, 40° and 60 °C using a digital density meter. The measurements are accurately described by the linear density relation (1) with the following densities at 20 °C and coefficients of thermal expansion: $\rho_{20} = 0.8784$ g cm^{-3}, $\alpha = 6.51 \times 10^{-4}$ °C^{-1} for 'Hyvis 3' and $\rho_{20} = 0.8964$ g cm^{-3}, $\alpha = 5.79 \times 10^{-4}$ °C^{-1} for 'Hyvis 30'. Finally, the coefficient of thermal diffusion is estimated from manufacturer's data and by comparison with the properties of many other oils to be $\kappa = 8 \times 10^{-4}$ cm^2 s^{-1} (± 20 %). Hence, the Prandtl numbers at 20 °C are $Pr = 1.2 \times 10^5$ and 1.8×10^6.

3.2. *Apparatus*

Thermals were created by injecting a known volume of heated oil into a large tank of the same oil at room temperature. The tank was 40 cm square and filled to a depth of 70 cm. The tank was insulated and kept in an air-conditioned room. Motions of this initially cold fluid due to the passage of a thermal were in many experiments made visible by injecting, before the run and at various heights, a number of horizontal lines of the same oil containing a small concentration of dye. These lines were injected from a syringe connected to a long vertical syringe tube that could be

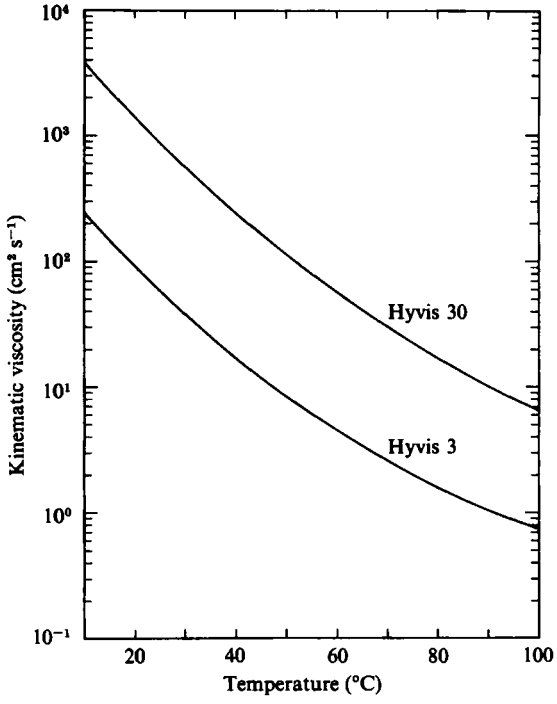

FIGURE 2. The kinematic viscosity of 'Hyvis 3' and 'Hyvis 30' as functions of temperature.

traversed slowly across the tank. Lines were positioned as close as possible to the axis of the tank, thus close to the axis of the thermal. These lines also served to reveal whether slow, large-scale convective motions due to a sidewall heat transfer were present.

Oil to be injected was dyed and preheated for several hours in a metal piston and cylinder arrangement that was surrounded by a hot-water jacket connected to a constant-temperature bath. In order to minimize heat transfer to the tank, the cylinder had to be disconnected from the tank at all times, excepting during injection of hot oil. Hence, one end of the cylinder could be pushed into a plastic 'source' in the base of the tank just before the injection. The source had a stop-cock and an injection hole 0.2 cm in diameter, which released the hot fluid at a level almost flush with the inner base. Release adjacent to the flat base was chosen as the simplest practical geometry (and one of general interest), given that a release far from the base would involve a long injection tube with significant thermal effects as well as unknown viscous effects on the subsequent flow. The volume injected into the tank was measured to an accuracy of 0.3 cm^3 directly from a calibration scale on the piston shaft and a correction was made for the small volume (0.25 cm^3) of the connecting passage.

3.3. *Procedure*

Before each experiment the oil in the tank was stirred as much as practicable with a rod in order to minimize any vertical temperature gradient that may have been produced by heat transfer to the room, though temperature measurements near top and bottom revealed no measurable difference. The temperature in the tank was measured to 0.1 °C before every experiment. Horizontal dye lines were then injected, if desired, and a photograph taken to record their initial positions. The piston and

cylinder containing hot dyed oil was then connected to the source in the base of the tank, and a desired volume of up to 36 cm^3 injected. Injection took only 5–10 s. A digital clock was started at the beginning of the injection. Thereafter, photographs of the flow as projected onto a shadowgraph screen on the front of the tank were taken at regular intervals. (Ciné films were also made of several experiments.) Photographs included the clock and a square gridscale on the shadowgraph screen. As soon as possible after the injection, the cylinder was disconnected from the tank, as it was found that a small quantity of heat conducted through the plastic source could cause flow in the tank after a period of an hour or so.

3.4. *Isothermal control experiments*

In order to provide a comparison with the thermals, experiments were also carried out with miscible drops possessing no temperature anomaly but a small compositional buoyancy. 'Hyvis 3' was mixed with a medicinal oil of low viscosity and smaller density in proportions such that the density of the mixture (at 20 °C) was 0.0106 g cm^{-3} less than that of 'Hyvis 3'. This mixture was then injected into the tank of 'Hyvis 3' using the same apparatus as for the other experiments, but at the same temperature as the oil in the tank. All liquids were completely miscible. The viscosity of the mixture was 4 $cm^2\ s^{-1}$, giving a viscosity ratio of 0.043. Two injection volumes were used, both giving sphere diameters less than one tenth the width of the tank. (Diameters of thermals ranged from 1–4 cm.) These isothermal experiments served to calibrate the apparatus, particularly the influences of the rigid base, free surface and the sidewalls of the tank.

4. Observations and definitions of measurements

Each injection produced a nearly spherical blob at the source. Initial momentum of the fluid leaving the small hole was dissipated within a few seconds and had no effect on the subsequent flow. Figure 3 shows the development of a thermal with $Ra = 1.65 \times 10^3$, $\Delta T_0 = 70.0$ °C and an initial viscosity ratio of 0.0125. As the hot oil rises away from the source, the blob first becomes tapered at the rear (figure 3*a*). A very small quantity of the dyed fluid cannot be carried away from the rigid base, and a trail connecting the source to the blob becomes longer and thinner with time. This trail exists throughout the experiment (though it usually becomes so thin as to be invisible) simply because motion on the axis of symmetry is continuous and purely vertical. It is important to realize that buoyant fluid does not continue to rise up to the thermal in the trail, as it does in the isothermal, continuous source experiments of Whitehead & Luther (1975) and Olson & Singer (1985). In the reference frame moving with the thermal (figure 1) there must be a stagnation point on the axis behind the thermal, and it is there that the trail becomes thinnest. Below this point, fluid is moving away from the thermal, though it is being pulled upward relative to the tank.

Soon after leaving the base, the rear of the dyed fluid is flattened, followed by the appearance of a cusp and the intrusion of non-dyed fluid (figure 3*b*). These are the first signs that ambient fluid is being entrained into the thermal. Once the cap (forward edge) of the thermal has reached some height, in this case four diameters from the source, the fluid with no dye has penetrated up to the cap and the dyed fluid is confined into an annular ring or torus (figure 3*c*).

The bright and dark bands on shadowgraph images indicate a large refractive-index gradient due to a large temperature gradient around the cap of the thermal. The

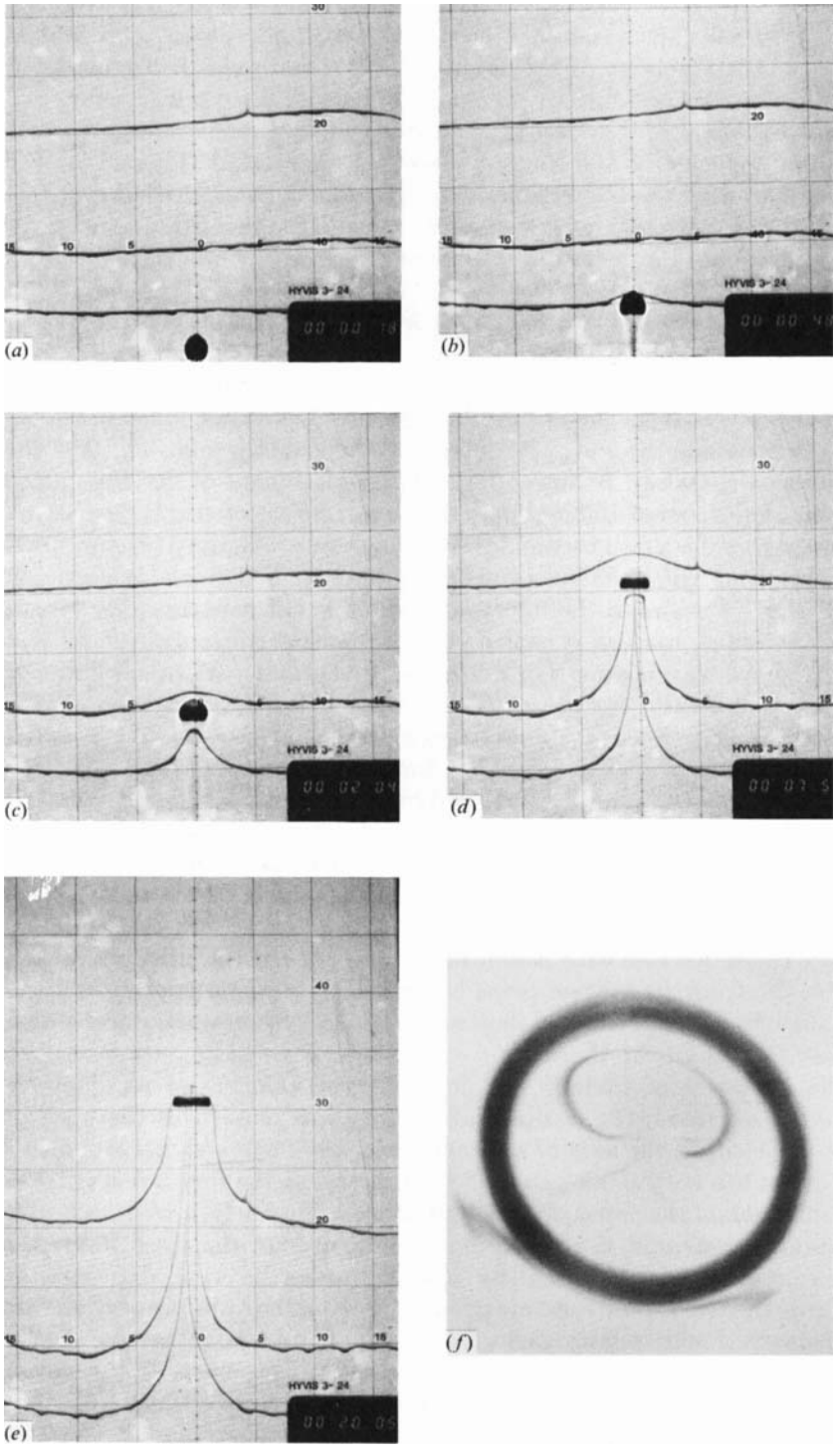

FIGURE 3. Shadowgraph images of a thermal in 'Hyvis 3' with $Ra = 1.65 \times 10^3$, $V_0 = 2.4$ cm^3, $\Delta T_0 = 70.0$ °C, and $\mu_0/\mu_\infty = 0.0125$. (*f*) is a plan view of the thermal when it is 40 cm from the source. Two dye lines are visible in (*f*), and apparent deviations from axisymmetry are a result of camera angle only. The Reynolds number based on initial velocity and diameter is 1.8×10^{-3}. A 5 cm square grid is drawn on the shadowgraph screen.

persistence of this gradient between the oncoming fluid and the non-dyed fluid inside the thermal in turn indicates that the entrained fluid, which soon makes up the greater part of the volume of the thermal, is hot and only distinguished from the injected fluid by the presence or otherwise of dye. A large temperature gradient is not visible at the rear of thermals because it is spread, rather than sharpened, by the inward radial velocity. When the bounds of the thermal at this and later stages of development are described by a spherical surface coincident with the large temperature gradient at the cap and slides, it is found that the centre of the torus of dyed fluid lies slightly above the horizontal equator of the sphere (i.e. in the forward hemisphere).

Figure 3(*d*) and (*e*) show later stages in the evolution, and the way in which horizontal dye lines lying sufficiently close to the axis are entrained. The lines rarely lie exactly on the axis and are therefore advected around the side of the thermal closest to or farthest from the camera. A segment of each line may enter the thermal boundary layer where the line approaches closest to the thermal. The first and second lines have been entrained in figure 3(*e*). The displacement of dye lines also shows a large vertical transport of ambient fluid that is not assimilated into the thermal. These displacements are discussed further in Griffiths (1986*a*). Figure 3(*f*) shows a plan view of the thermal, in which the torus of dye is obvious. This torus is simply a passive 'chemical ring' containing the injected fluid. It is not a vortex ring (vorticity has diffused to infinity), nor can it contain any significant concentration of heat.

Figure 4 shows varius stages in the rise of a thermal with much larger Rayleigh number ($Ra = 9.1 \times 10^3$, $\mu_0/\mu_\infty = 0.0125$). Qualitative features of the flow are the same as for the experiment in figure 3, excepting that the sharp temperature front around the thermal shows no signs of diminishing throughout the thermal's rise through the depth of the tank. All three dye lines are entrained and their circulation inside the thermal could be traced. By way of contrast, figure 5 shows two stages during an experiment with $Ra = 312$ using 'Hyvis 30'. The flow at this smaller Rayleigh number is characterized by greater elongation of the cross-section of the torus, which is also farther from the equator of a fitted sphere (see Griffiths 1986*a*), and a more rapid increase with height of the diameter of the thermal. As at all other conditions, the front stagnation point is marked by a small amount of dyed fluid at the junction of a thin line of dyed fluid along the axis of symmetry and a thin surface of dye over the cap of the thermal.

For the purposes of finding the position and velocity of thermals from the photographic sequence, the position of the cap was defined as the position of the temperature front on the axis of symmetry or, when this was not sufficiently clear, the position of the very small patch of dye trapped at the forward stagnation point. Thus the position of the cap is always well defined. Similarly, a well-defined diameter that is readily measured is the maximum diameter of the dyed fluid. While this dimension must always be slightly smaller than the true diameter based on temperature, the two should remain approximately in the same proportion throughout an experiment. Each measurement of position and diameter was corrected for parallax errors arising from the distances from the light source to the thermal (7 m) and the thermal to the shadowgraph screen (20 cm). Measurements taken after the cap of the thermal has approached to within three diameters from the free surface were discarded as the proximity of the surface caused more rapid horizontal spreading.

Figure 6 shows shadowgraph photographs of an isothermal control experiment using the less dense mixture of 'Hyvis 3' and medicinal oil. In this case, any diffusion

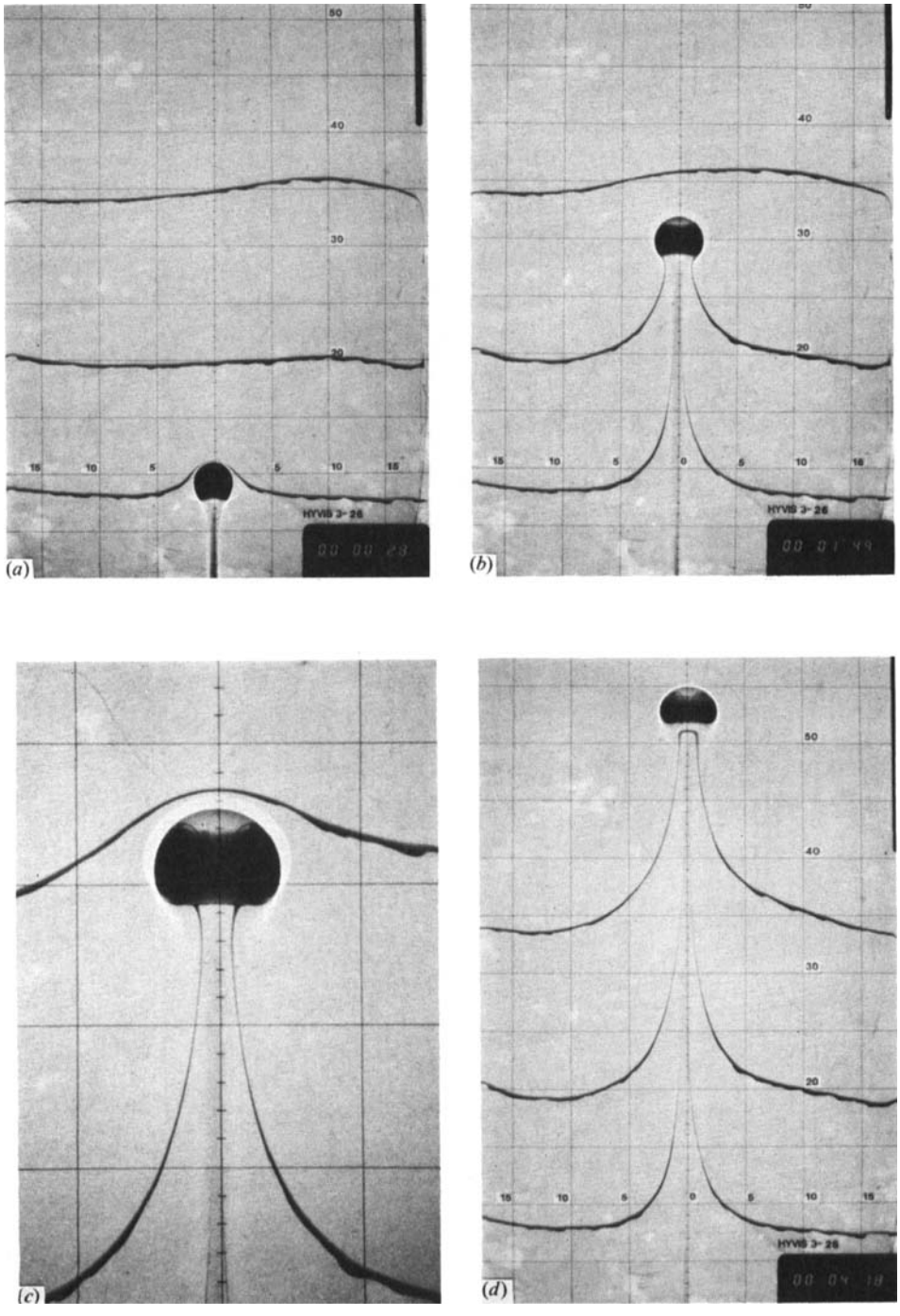

FIGURE 4. Shadowgraph images of a thermal in 'Hyvis 3' with $Ra = 9.10 \times 10^3$, $V_0 = 13.0$ cm^3, $\Delta T_0 = 70.0$ °C and $\mu_0/\mu_\infty = 0.0125$. The enlarged view in (*c*) was taken 140 s after injection when the cap is 37.7 cm above the base of the tank. The Reynolds number based on the initial velocity and diameter is 9.8×10^{-3}.

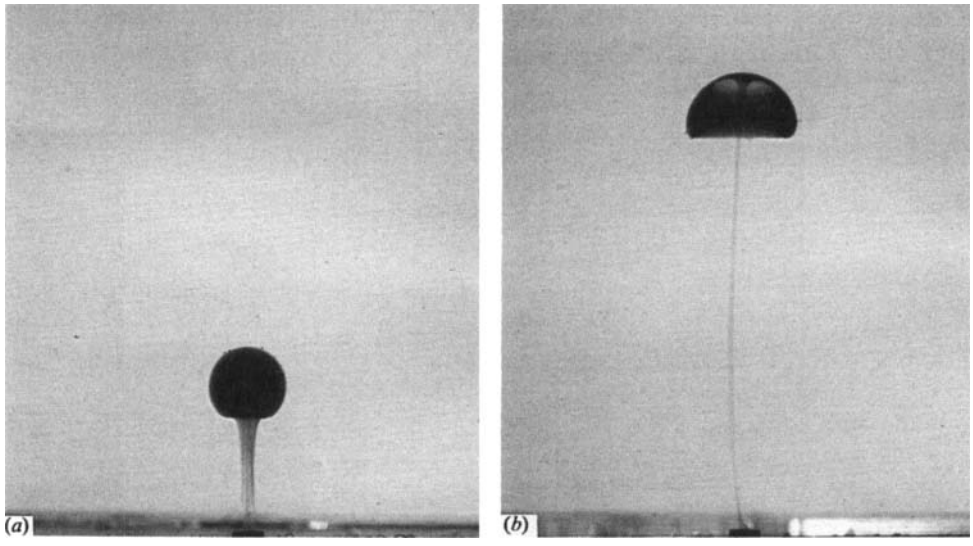

FIGURE 5. Photographs of a thermal in 'Hyvis 30' (silhouetted against a bright background) with $Ra = 312$, $V_0 = 20.5$ cm^3, $\Delta T_0 = 48.7$ °C, $\mu_0/\mu_\infty = 0.024$. The initial Reynolds number is 2.8×10^{-5}. Photographs were taken (*a*) 3 min 30 s and (*b*) 26 min 33 s after injection.

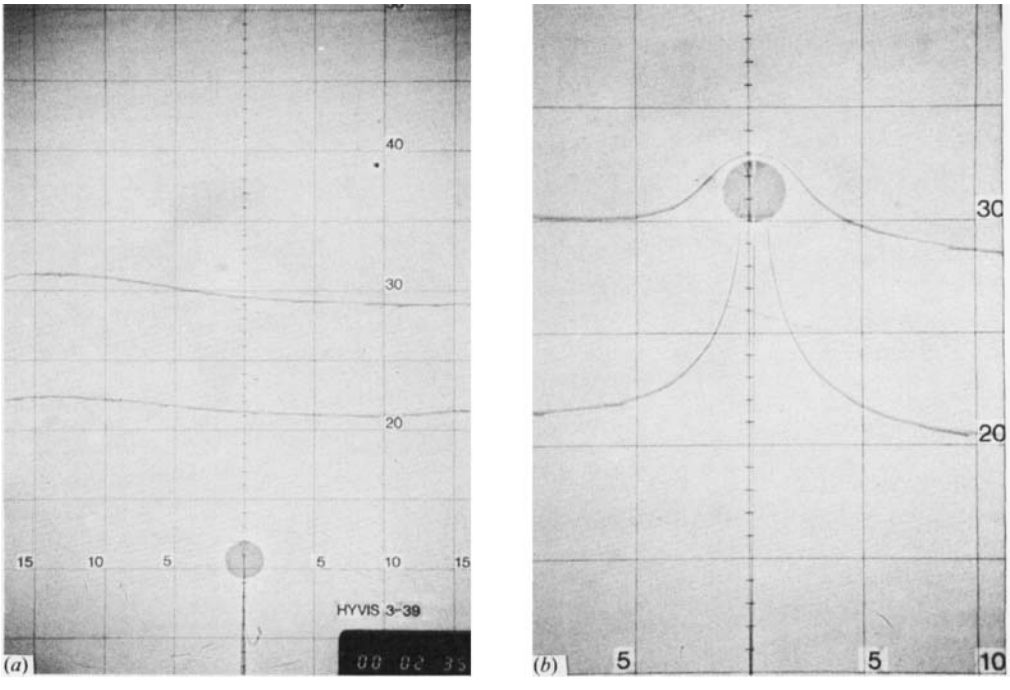

FIGURE 6. Shadowgraph images of an isothermal bubble of miscible fluid for which there is practically no diffusion of buoyancy over the length- and timescales of the experiment. $\Delta\rho = 0.0106$ g cm^{-3}, $V_0 = 11.3$ cm^3, $\nu_\infty = 90$ cm^2 s^{-1}, $\mu_0/\mu_\infty \approx 0.04$ and $Re = 2.0 \times 10^{-3}$. The effective Rayleigh number based on the chemical diffusion coefficient is of order 10^8.

of buoyancy is insignificant within the duration of the experiment since the species diffusion coefficient is several orders of magnitude smaller than that of heat. No significant entrainment occurs and the injected fluid remains within a spherical bubble throughout the depth of the tank. Some weak striations visible inside the bubble are a result of a small amount of mixing during injection, and serve nicely to reveal the shape of circulation inside the sphere. These bubbles did not slow down, whereas entraining thermals often became so slow before reaching the top of the tank that measurements were terminated because there was a risk that the thermal might have begun to be carried by undetectably slow, large-scale convective motions which might have been present.

5. Experimental results

5.1. *Height of rise and velocity of thermals*

The measured position of each thermal is plotted against time in figure 7. Here z_L is the height of the cap above the base of the tank, t_L is the time as recorded on the clock and $z' = z_L(t_L = 0)$. The latter position was found by plotting $z_L(t_L)$ on linear scales and extrapolating a straight-line fit to the first four measurements a short distance back to $t_L = 0$. Since the clock was started at the time of injection, z' is always close to one diameter D_0. The experiments have been separated according to their initial temperature anomaly, since the corresponding differences in viscosity ratio were expected to cause small differences in behaviour. The Rayleigh number and initial volume for each experiment are given in table 1. The positions of two isothermal buoyant bubbles are also plotted, along with the best fit of constant velocity for these two trajectories and the theoretical trajectory given by Stokes' law for the case $\mu/\mu_0 \ll 1$ in an unbounded fluid.

Isothermal bubbles rise throughout the depth of the tank with no significant deviation from a constant velocity, excepting for a decrease in velocity within two diameters of the free surface. No variation of velocity can be detected as the drop moves away from the vicinity of the rigid base. However, their velocity throughout the tank is 22 % smaller than that predicted by Stokes' law (3) for the appropriate viscosity ratio. Given that bubble diameters are 2.4 cm and 2.8 cm, or 0.07 times the width of the tank, a velocity deficit of close to 20 % is expected to result from an increased drag associated with the presence of the sidewalls†. Effects of interfacial tension and interfacial impurities are a further possible cause of the measured velocity deficit, since finite interfacial tensions are possible at sharp interfaces, even between two miscible fluids. The effects of interfacial tension on isothermal miscible drops of corn syrup/water mixtures are discussed by Kojima *et al.* (1984), where tensions for drop diameters an order of magnitude smaller, and velocities much larger, than those used here are inferred to be three orders of magnitude smaller than that appropriate to an air–water interface. Tensions decrease with decreasing velocity because diffusion smears the interface. In the present experiments, the large drop diameters and small velocities strongly suggest that interfacial effects are negligible, a conclusion supported by observations in other experiments using the same oils (Griffiths 1986*b*), where an extremely thin spherical film forms over the forward hemisphere of thermals with combined compositional and thermal buoyancies. Hence

† The exact influence of sidewalls was not computed for the square box. Rather, the above figure is based on Happel & Brenner's (1965) analysis for a rigid sphere moving along the axis of a cylinder (giving a 17 % velocity deficit) and on double the drag experienced by a body moving along the mid-plane between two parallel walls (giving a 22 % velocity deficit).

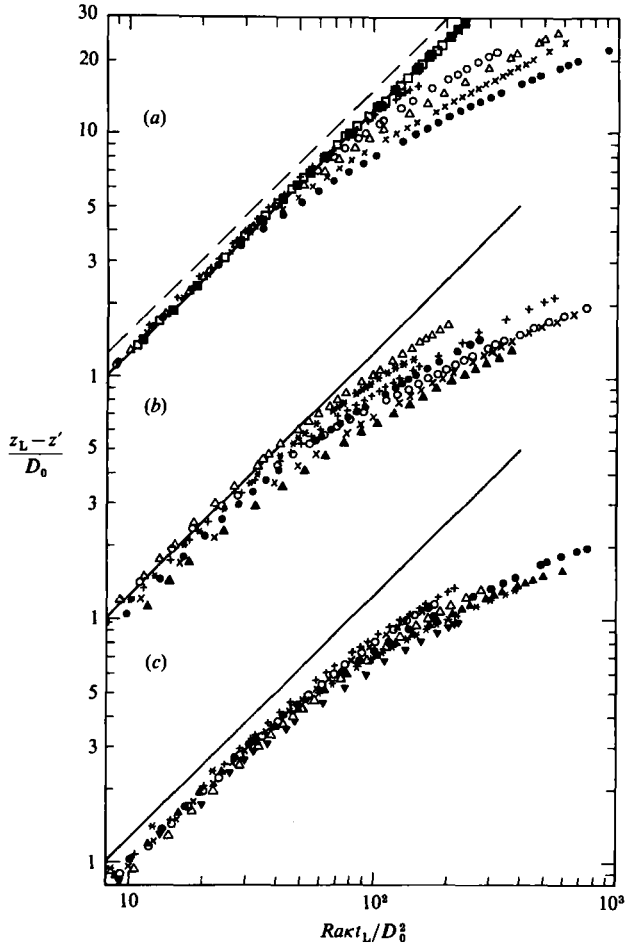

FIGURE 7. Vertical position of thermals and isothermal bubbles as functions of dimensionless time. Height of the cap is measured from the initial position z' at $t_L = 0$, where t_L is the time on the laboratory clock. Results are shown for three initial temperature anomalies (*a*) 70 °C, (*b*) 40 °C and (*c*) 20 °C. The injected volume and Rayleigh number for each experiment are given in table 1. Data for isothermal bubbles are shown in (*a*) (filled and open squares) and are well described by a trajectory of constant velocity (solid line). This velocity is 22% smaller than that predicted by Stokes' law for a sphere with $\mu/\mu_\infty \ll 1$ in an unbounded fluid (broken line). The solid line is reproduced in (*b*) and (*c*) for reference. The velocity of thermals decreases with time more rapidly for smaller Rayleigh numbers.

the discrepancy from Stokes' law is treated entirely as a calibration of the effects of the finite size of the tank and the velocity of thermals will be compared to the measured rather than theoretical velocity of isothermal bubbles.

While thermals are within three to four diameters from their initial position they rise with a nearly constant velocity. For all thermals with initial temperature anomaly of 70 °C ($\mu_0/\mu_\infty = 0.0125$), this initial velocity is equal to that of the isothermal bubbles (for which $\mu/\mu_\infty \approx 0.04$). The same is true for the largest of those thermals with $\Delta T_0 \approx 40$ °C ($\mu_0/\mu_\infty \approx 0.05$). This result is consistent with Stokes' law, which predicts that the rise velocity is effectively independent of viscosity ratio for $\mu/\mu_\infty \ll 1$. Smaller thermals with $\Delta T_0 \approx 40$ °C begin to rise with velocities 5–10% smaller than low-viscosity bubbles, while thermals with $\Delta T \approx 20$ °C

ΔT_0 (°C)	Symbol	V_0 (cm^3)	*Ra*
~70°	+	36.0	2.5×10^4
	○	13.0	9.1×10^3
	△	6.0	4.2×10^3
	×	2.5	1.85×10^3
	●	2.4	1.65×10^3
~40°	△	30.0	1.2×10^4
	*	22.7	7.9×10^3
	▼	13.2	4.6×10^3
	+	8.0	3.26×10^3
	●	8.2	2.9×10^3
	○	4.5	1.75×10^3
	×	3.5	1.22×10^3
	▲	2.3	7.9×10^2
~20°	+	36.0	1.12×10^4
	○	24.7	5.4×10^3
	×	24.7	5.4×10^3
	△	11.9	2.65×10^3
	●	12.5	2.50×10^3
	▲	7.4	1.16×10^3
	*	4.9	7.6×10^2
	▼	1.2	2.5×10^2

TABLE 1. Rayleigh numbers *Ra* and injected volume V_0 for each experiment. Three nominal temperature anomalies were used, but the precise temperature difference used to calculate *Ra* differs from the nominal value by up to 0.3 °C. The absolute temperature in the tank was in every case close to 20°. Hence, the temperature difference of 70 °C corresponds to a viscosity ratio $\mu_0/\mu_\infty = 0.0125$, $\Delta T_0 \sim 40$ °C to $\mu_0/\mu_\infty \approx 0.05$ and $\Delta T_0 \sim 20$ °C to $\mu_0/\mu_\infty = 0.16$–0.20. Symbols are defined from figures 7, 8, 9 and 11

($\mu_0/\mu_\infty = 0.16$–0.20) have initial velocities as much as 20% smaller. Allowing for an increase in viscosity ratio due to the more rapid cooling of smaller and slower thermals, these velocities too are consistent with Stokes' law.

The initial constant velocity regime coincides with the period during which the structure of thermals is first developing and during which the rigid base may strongly influence the flow, hence the shape of the buoyant fluid. The first entrained fluid reaches the cap only near the end of this period, indicating that circulation within the sphere has undergone only $\frac{1}{2}$–1 turnovers and that the flow is unlikely to be self-similar. At the same time, it is a surprise to find that the proximity of the rigid base has no significant influence on the velocity of either isothermal bubbles or thermals. This does not necessarily imply that the base has no influence on the flow, rather that any variation with height of the additional drag on the buoyant fluid appears to be off-set by a changing shape of the bubble at small times. The motion of a liquid drop away from a wall requires further analysis.

At larger times, the velocities of thermals decrease with time, the rate of decrease being greater for smaller Rayleigh numbers. Trajectories appear to approach the power law $z_L - z' \sim t_L^{\frac{1}{2}}$. However, we cannot be certain of this behaviour from figure 7 as the height z_L is an integrated property of the flow and as the virtual origins (judging from the slow rate of expansion of thermals, to be discussed later) must lie a large distance below the source. A test of the similarity solution presented in §2 is best constructed by first locating the virtual origin in time for each thermal. Since

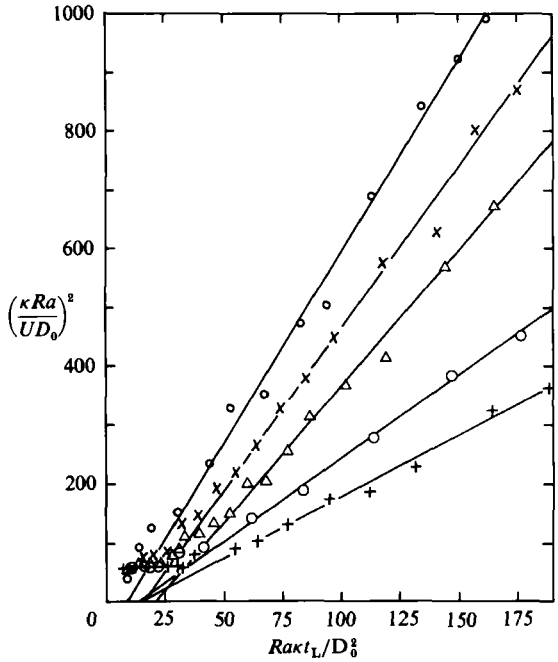

FIGURE 8. Inverse square of velocity for a number of thermals as a function of time. No assumption about the location of a virtual origin is required when fitting the power law of (12) (straight lines). Extrapolation to $U^{-2} = 0$ gives the virtual original in time. Data are for $\Delta T_0 = 70$ °C. Rayleigh numbers are given in table 1.

the velocity is an instantaneous property of the flow, we can plot on linear scales the inverse square of the dimensionless velocity as a function of the dimensionless laboratory time t_L. The choice of the inverse square is suggested by (12). Some examples are shown in figure 8. Velocities are computed by taking the difference between successive measurements of the position z_L, and therefore show considerable scatter. However, the results for all thermals show that there is a rapid transition from an initial regime of adjustment toward self-similar flow and motion away from the rigid base with nearly constant velocity, to one in which $U^{-2} \sim t_L$. Hence, $U \sim (t_L - t^*)^{-\frac{1}{2}}$, where the virtual origin at $t_L = t^*$ is found by extrapolating the straight lines of best fit backward to $U^{-2} = 0$ (as shown in figure 8). Because the form (12) gives large velocities near the virtual origin, the origin in time is not far from the time of injection.

In figure 9, the trajectories of figure 7 are plotted again, this time on linear axes and with the height $(z_L - z')/D_0$ as a function of the square root of time measured from the virtual origin. Though the trajectory of isothermal bubbles has no virtual origin, it is adjusted to be at the same height as are thermals at $t_L - t^* = 0$ and plotted here for reference. After the initial adjustment period (which we neglect), thermals are well described by the form (13) with $t = t_L - t^*$ (the straight lines on figure 9). Some experiments show a further decrease in velocity at large times, possibly as a result of an increasing sidewall influence as the diameter of thermals increases, or to a slow but cumulative loss of heat from the thermal. The slopes m of the straight lines in figure 9 are plotted against the Rayleigh number in figure 10. The power law of best fit is found to be $m \sim Ra^{0.24 \pm 0.03}$. Since this result supports the predicted form $m = qRa^{\frac{1}{4}}$ in (13), where $q = f/\pi C$, it is justified to find the $\frac{1}{4}$-power law of best fit:

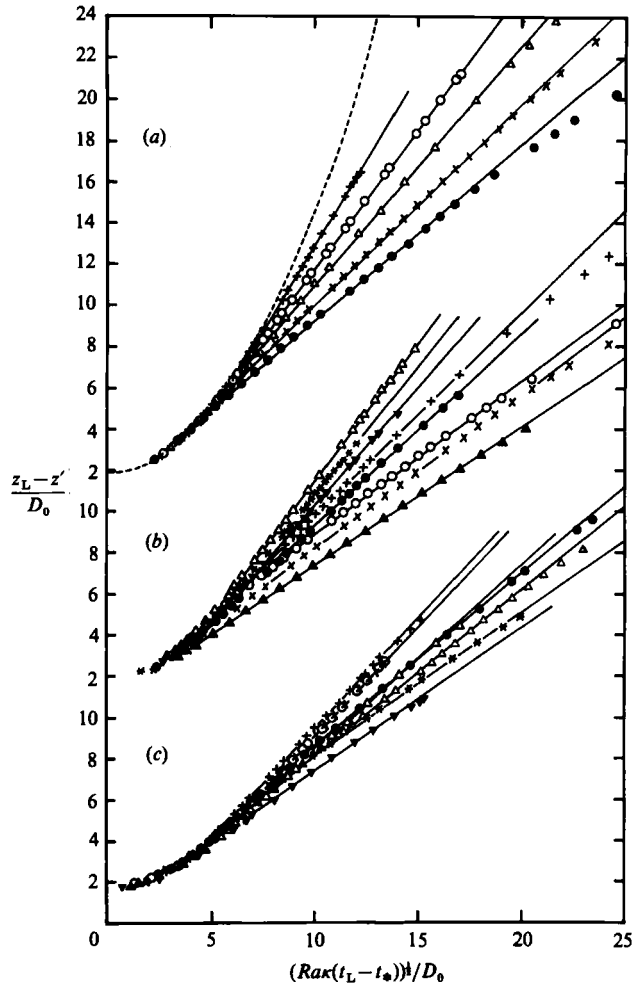

FIGURE 9. Trajectories of thermals from figure 7, plotted as functions of the square root of the dimensionless time $t_L - t^*$, which is the time from the virtual origin. (*a*) $\Delta T_0 \approx 70°$, (*b*) $\Delta T_0 \approx 40°$, (*c*) $\Delta T_0 \approx 20$ °C. The Rayleigh number for each experiment is given in table 1. Straight lines show that the data are described satisfactorily by the $t^{\frac{1}{2}}$ law when $(z_L - z')/D_0 > 5$. For reference, the parabola in (*a*) shows the trajectory (starting from $t_L - t^* = 0$) for bubbles with a constant velocity.

$m = (0.14 \pm 0.01)\, Ra^{\frac{1}{4}}$ (solid line on figure 10). In fact, two values of q differing by approximately 10 % are found when the data obtained for a temperature anomaly of 70 °C are considered independently from the data for the smaller temperature anomalies. The highest value is expected to describe the limit $\mu/\mu_\infty \to 0$, where $f = 1$. Using this value of q, and including a systematic uncertainty of 30 % in the Rayleigh number due to uncertainties in total buoyancy and molecular properties, the constant C is evaluated as $C \approx 2.0 \pm 0.4$.

5.2. *Angle of expansion*

The diameters of thermals are plotted in figure 11 as functions of the vertical position z_L of the cap. The diameter D is that measured from the photographic record, while the scaling length D_0 is that calculated for a sphere with the measured injection

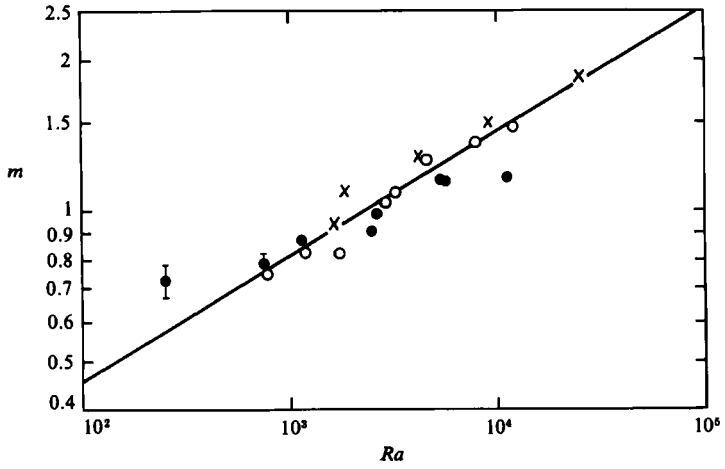

FIGURE 10. Slopes m of the straight lines on figure 9 plotted against the Rayleigh number. The slope m is the coefficient for the solution (13). The straight line is $m = 0.144\,Ra^{\frac{1}{3}}$. Data are distinguished according to the initial temperature anomaly: ×, $\Delta T_0 = 70°$; ●, $\Delta T_0 \approx 40°$; ○, $\Delta T_0 \approx 20\,°C$.

volume. For the isothermal bubbles these two measurements gave $D/D_0 = 0.95$–0.98, values that remained constant until the bubble approached to within two diameters of the free surface.

While within four to six diameters of the source, thermals are not spherical and undergo variations of diameter that appear to depend upon both the Rayleigh number and the viscosity ratio. These variations are probably due to the influence of the base of the tank and the adjustment toward self-similar flow. At later times, the results for most thermals are reasonably described by straight lines and therefore support the similarity solution (15)†. The absolute values of D during this period appear to depend upon the details of the early adjustment phase. From figure 11 it is seen that thermals with smaller Rayleigh numbers expand more rapidly with height than do thermals with larger Rayleigh numbers. The measured expansion rates ϵ are plotted against the Rayleigh number on figure 12. The power law of best fit is $\epsilon = 0.63\,Ra^{-(0.44\pm0.1)}$. Since this result is consistent with (15) we fit the predicted $\frac{1}{2}$-power law to find $\epsilon = (1.25\pm0.2)\,Ra^{-\frac{1}{2}}$ and $C = 0.9\pm0.3$. Although the above value for C is of the same order as that found from the velocity and height of thermals, it is worth evaluating the constant as precisely as possible. The value determined directly from measurements of the expansion rate is likely to be the more reliable of the two as it does not rely upon the consistency argument used in locating a virtual origin and plotting the trajectories in figure 9. On the other hand, expansion rates may have been slightly underestimated since the measured visible diameter of the dye ring at large times is likely to be up to 20% smaller than the actual diameter of the buoyant material. With these difficulties in mind, the value $C \approx 1$ is the best estimate available from the present data.

† The rate of expansion of an isothermal slender toroidal ring resulting from inertial effects, as found to leading order in Reynolds number by Kojima *et al.* (1984), would give $\epsilon \sim Re = 10^{-5}$–$10^{-3}$. This expansion is much smaller than that observed for thermals, where some of the largest expansion rates are found for the smallest Reynolds numbers.

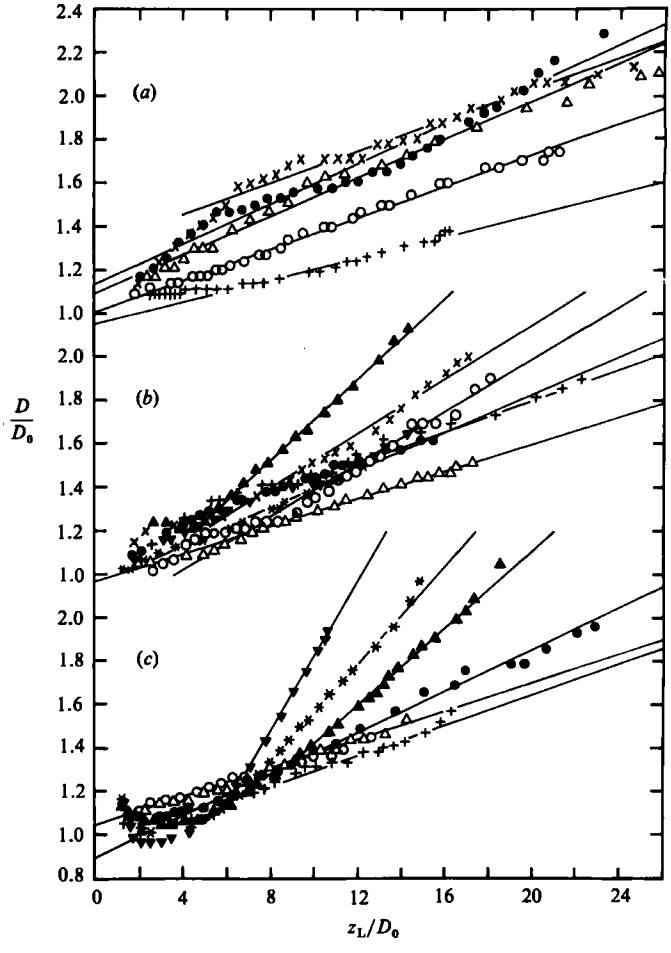

FIGURE 11. Diameters of thermals as measured from their shadowgraph images and normalized by D_0, as functions of the vertical distance from the source to the cap. Results for each initial temperature anomaly are shown separately as they involve different viscosity ratios: (*a*) $\Delta T = 70°$; (*b*) $\Delta T \approx 40°$; (*c*) $\Delta T \approx 20$ °C. Rayleigh numbers are given in table 1. For most thermals, data are consistent with a straight line when $z_L > 5$.

6. Conclusions and application

The flow induced by a given localized quantity of thermal buoyancy is considered for the case in which both the Prandtl number for the fluid and the Rayleigh number are large compared to one but $Ra \ll Pr$. Under these conditions, motion is characterized by a small Reynolds number. Since the flow is dominated by advection, the diffusion of heat causes only a negligible modification of the instantaneous flow field given by the solution for reversible flow around a spherical drop. Rapid diffusion of vorticity also ensures that the flow at any time is described by the steady Stokes solution, despite the slow time-dependence produced by thermal diffusion. A thin thermal boundary layer becomes buoyant on being heated, and is consequently assimilated into the 'thermal'. The resulting evolution and motion of the thermal are well described by a straightforward similarity solution with one empirically evaluated constant. The laminar entrainment leads to a continuous increase of the volume of

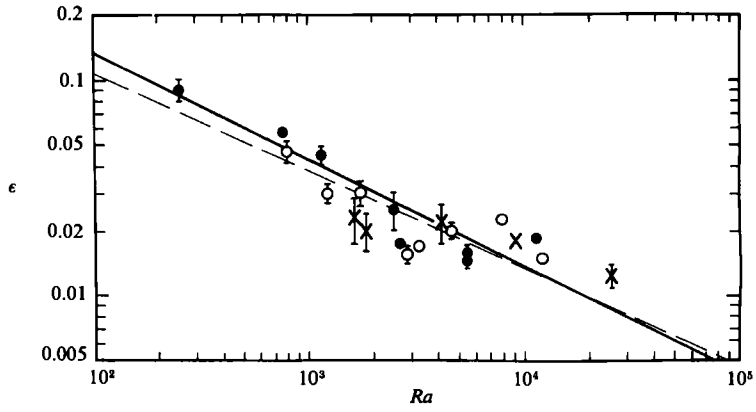

FIGURE 12. Expansion rates ϵ for the radius of thermals as given by the slope (divided by two) of the straight lines in figure 11, as a function of Rayleigh number. The broken line is the power law of best fit and has slope -0.44. The solid line is $\epsilon = 1.25\,Ra^{-\frac{1}{2}}$. Data are distinguished according to the initial temperature anomaly: ×, $\Delta T_0 = 70°$; ●, $\Delta T_0 \approx 40°$; ○, $\Delta T_0 \approx 20$ °C.

buoyant material in such a way that the diameter is directly proportional to the height through which the thermal has risen. Entrainment also leads to a reshaping of the fluid that makes up the spherical thermal at any time – it becomes a torus of ever-increasing radius. This dye ring must not be mistaken for either a vortex ring or a concentration of heat, despite its qualitative similarity in appearance and evolution to large Reynolds number vortex rings, for it simply marks the location of the initially buoyant fluid.

A major assumption of the model is that all of the heat in the boundary layer is entrained, conserving the total buoyancy of the thermal and preventing the formation of a warm trail. A more general solution allowing some loss of heat into a thermal wake can be formulated but has two numerical constants to be empirically evaluated and it cannot be compared unambiguously with the existing data. On the other hand, physical reasoning suggests that only a small heat loss is likely from the outer wing of the diffusive boundary, and the solution with constant buoyancy provides a satisfactory description of our experimental results. An ever-thinning trail of warm and dyed fluid is observed to stretch from the source to the thermal, but this does not imply a heat loss from the thermal. The trail is simply a result of the initial conditions, and can never be broken. The empirical value of the numerical constant $C \approx 1$ implies that the unknown proportionalities in the expressions for the boundary-layer thickness (4) and volume flux (5) satisfy $k_1 k_2 \approx 2$, a result that is consistent with the conclusion that practically all of the warm boundary layer is entrained.

The similarity solution and experimental results for extremely viscous thermals with large Rayleigh numbers ($2.5 \times 10^2 < Ra < 2.5 \times 10^4$) are significantly different from previous results for weak thermals ($Ra \to 0$) and for turbulent thermals. Thermals at $Ra \to 0$ are predicted to increase in size according to $D \sim Ra^{-1}z$, while inviscid vortex rings are found to enlarge at an angle independent of the Rayleigh number. The results reported here give $D \sim Ra^{-\frac{1}{2}}z$. Similarly, the height risen by thermals is $z \sim Rat^{\frac{1}{2}}$ at $Ra \to 0$, $z \sim Ra^{\frac{1}{4}}t^{\frac{1}{2}}$ for large Reynolds numbers, and $z \sim Ra^{\frac{3}{5}}t^{\frac{1}{2}}$ for the present conditions ($Re \ll 1$, $Ra \gg 1$). It is interesting to note that the data of Schlien & Thompson (1975) for thermals with $Ra = 10^3$–10^4 and $Re \approx 20$ suggest

the distance travelled is proportional to $Ra^{\frac{1}{2}}$, a behaviour intermediate to those now established for small and large Reynolds numbers. However, the latter result is uncertain because the effect on the trajectory of a separation of source and virtual origin was not considered.

The effects of large viscosity variations are of particular interest. A strongly temperature-dependent viscosity simply results in a smaller rate of viscous dissipation inside thermals and a translation velocity as much as 25% larger than that expected in an isoviscous fluid. The model presented here is not in principle restricted to single-state flow and can be applied (perhaps with a modification for latent-heat effects) to describe the behaviour of a mass of molten material such as magma pushing upward through a viscous solid. The model requires only that $1 \ll Ra < Pr$ and that density differences are due to temperature differences alone. Finally, the model and observations presented here are relevant to studies of thermal convection in very viscous fluids such as the Earth's solid mantle and liquid magma stored in magma chambers. The results are employed in an accompanying article (Griffiths 1986*a*) in order to predict motions induced in the surrounding fluid by a thermal and to further explore the formation of the toroidal ring. Implications for motions of individual isolated thermals (or 'diapirs') in the mantle will be discussed in detail elsewhere (Griffiths 1986*c*). The model is also applicable to solute-driven convection in water if the diffusion coefficient for heat is replaced with a solute diffusion coefficient and the density variation due to thermal expansion is replaced by the solutal density difference. Since solute diffusion coefficients are at least two to three orders of magnitude smaller than that of heat, the effective Prandtl (Schmidt) number is large ($\sim 10^3$) even in aqueous solutions of small viscosity. The regime $1 \ll Ra < Pr$ (giving $Re < 1$) is therefore of interest for small droplets of solute-laden water sinking through a relative freshwater environment (or relatively fresh droplets rising through a salty environment) as occurs below (and above) double-diffusive salt-finger interfaces. The expansion of thermals and formation of toroidal rings at small Reynolds numbers also imply that aggregates of suspended particulate matter within viscous drops will be more effectively dispersed when there is a significant temperature difference between the drops and the surrounding fluid.

The experiments were made possible by the excellent technical assistance of Mr J. Micallef and photographic assistance of Mr R. Wylde-Browne.

REFERENCES

BATCHELOR, G. K. 1967 *An Introduction to Fluid Dynamics*. Cambridge University Press.

BRIGNELL, A. S. 1975 Solute extraction from an internally circulating spherical liquid drop. *Intl J. Heat Mass Transfer* **18**, 61–68.

CHU, T. Y. & GOLDSTEIN, R. J. 1973 Turbulent convection in a horizontal layer of water. *J. Fluid Mech.* **60**, 141–159.

ELDER, J. W. 1968 The unstable thermal interface. *J. Fluid Mech.* **32**, 69–96.

ESCUDIER, M. P. & MAXWORTHY, T. 1973 On the motion of turbulent thermals. *J. Fluid Mech.* **61**, 541–552.

FOX, D. G. 1972 Numerical simulation of three-dimensional, shape-preserving convective elements. *J. Atmos. Sci.* **29**, 322–341.

GRIFFITHS, R. W. 1986*a* Particle motions induced by spherical convective elements in Stokes flow. *J. Fluid Mech.* **166**, 139–159.

GRIFFITHS, R. W. 1986*b* The differing effects of compositional and thermal buoyancies on the evolution of mantle diapirs. *Phys. Earth Planet. Inter.* (submitted).

GRIFFITHS, R. W. 1986*c* Dynamics of mantle thermals with constant buoyancy or anomalous internal heating. *Earth Planet. Sci. Lett.* in press.

HAPPEL, J. & BRENNER, H. 1965 *Low Reynolds Number Hydrodynamics*, pp. 298–341. Prentice-Hall.

HOWARD, L. N. 1964 Convection at high Reynolds numbers. In *Proc. 11th Intl Congress Appl. Mech.*, Munich (ed. H. Gortler), pp. 1109–1115. Springer.

JARVIS, G. T. 1984 Time-dependent convection in the Earth's mantle. *Phys. Earth Planet. Inter.* **36**, 305–327.

KOJIMA, M., HINCH, E. J. & ACRIVOS, A. 1984 The formation and expansion of a toroidal drop moving in a viscous fluid. *Phys. Fluids* **27**, 19–32.

KRONIG, R. & BRINK, J. C. 1951 On the theory of extraction from falling droplets. *Appl. Sci. Res.* **A2**, 142–151.

LAMB, H. 1932 *Hydrodynamics*. Dover.

LOPER, D. E. & STACEY, F. D. 1983 The dynamical and thermal structure of deep mantle plumes. *Phys. Earth Planet. Inter.* **3**, 304–317.

MARSH, B. D. 1982 On the mechanics of igneous diapirism, stoping and zone melting. *Am. J. Sci.* **282**, 808–855.

MARSH, B. D. 1984 Mechanics and energetics of magma formation and ascension. In *Explosive Volcanism: Inception, Evolution and Hazards*, pp. 67–83. Washington: National Academy Press.

MARSH, B. D. & KANTHA, L. H. 1978 On the heat and mass transfer from an ascending magma. *Earth Planet. Sci. Lett.* **39**, 435–443.

MORGAN, W. J. 1971 Convection plumes in the lower mantle. *Nature* **230**, 42–43.

MORRIS, S. 1982 The effects of a strongly temperature dependent viscosity on slow flow past a hot sphere. *J. Fluid Mech.* **124**, 1–26.

MORTON, B. R. 1960 Weak thermal vortex rings. *J. Fluid Mech.* **9**, 107–118.

MORTON, B. R., TAYLOR, G. I. & TURNER, J. S. 1956 Turbulent gravitational convection from maintained and instantaneous sources. *Proc. R. Soc. Lond.* A **234**, 1–23.

OLSON, P. & SINGER, H. 1985 Creeping plumes. *J. Fluid Mech.* **158**, 511–531.

PAN, F. Y. & ACRIVOS, A. 1968 Heat transfer at high Peclet number in regions of closed streamlines. *Intl J. Heat Mass Transfer* **11**, 439–444.

RIBE, N. M. 1983 Diapirism in the Earth's mantle: experiments on the motion of a hot sphere in a fluid with temperature dependent viscosity. *J. Volcanol. Geothermal Res.* **16**, 221–245.

SCHLIEN, D. J. & THOMPSON, D. W. 1975 Some experiments on the motion of an isolated laminar thermal. *J. Fluid Mech.* **72**, 35–47.

SCORER, R. S. 1957 Experiments on convection of isolated masses of buoyant fluid. *J. Fluid Mech.* **2**, 583–594.

SCORER, R. S. 1978 *Environmental Aerodynamics*. John Wiley.

SPARROW, E. M., HUSAR, R. B. & GOLDSTEIN, R. J. 1970 Observations and other characteristics of thermals. *J. Fluid Mech.* **41**, 793–800.

TRITTON, D. J. 1985 Experiments on turbulence in geophysical fluid dynamics. 2. Convection in a very viscous fluid. In *Turbulence and Predictability in Geophysical Fluid Dynamics and Climate Dynamics*, pp. 193–199. Bologna: Soc. Italiana di Fisica.

TURNER, J. S. 1957 Buoyant vortex rings. *Proc. R. Soc. Lond.* A **239**, 61–75.

TURNER, J. S. 1964 The dynamics of spheroidal masses of buoyant fluid. *J. Fluid Mech.* **19**, 481–490.

TURNER, J. S. 1973 *Buoyancy Effects in Fluids*. Cambridge University Press.

WHITEHEAD, J. A. & LUTHER, D. S. 1975 Dynamics of laboratory diapir and plume models. *J. Geophys. Res.* **80**, 705–717.

YUEN, D. A. & SCHUBERT, G. 1976 Mantle plumes; a boundary layer approach for Newtonian and non-Newtonian temperature-dependent rheologies. *J. Geophys. Res.* **81**, 2499–2510.